Barrier tuning of atomic layer deposited Ta_2O_5 and Al_2O_3 in double dielectric diodes

Running title: Barrier tuning of ALD Ta_2O_5 and Al_2O_3

Running Authors: Nemr Noureddine *et al.*

Ibrahim Nemr Noureddine

Naser Sedghi

Ivona Z. Mitrovic

Steve Hall[a)]

University of Liverpool, Department of Electrical Engineering and Electronics, Brownlow Hill, L69 3GJ Liverpool, United Kingdom

[a)] Electronic mail: s.hall@liv.ac.uk

The performance of ultrathin atomic layer deposited dielectrics of low (Al_2O_3) and high (Ta_2O_5) electron affinity (χ) is investigated in metal-insulator-(insulator)-metal [MI(I)M] diodes. The conduction mechanisms in 4 nm thick atomic layer deposited Al_2O_3 and Ta_2O_5 single barrier MIM diodes are first studied to show the dominance of tunneling and thermally activated Poole–Frenkel emission respectively in these oxides. Varying the

layer thickness of Ta_2O_5 with a 1 nm thick layer of Al_2O_3 shows evidence for resonant tunneling in double barrier MIIM structures and is correlated with the simulated bound states in the quantum well formed between the two dielectrics. These findings demonstrate experimental work on barrier tuning of resonant tunneling diodes with sufficient rectifying capability at a turn-on voltage as low as 0.32 V enabling their potential use in terahertz applications.

I. INTRODUCTION

Diodes based on tunneling through one or more insulator layers are attractive rectifying devices for electronics and energy harvesting applications at terahertz (THz) and infrared (IR) frequencies[1] offering rectification into these regimes due to their short tunneling transit time in the range of femtoseconds.[2] Due to their ultrafast operation, these diodes are of interest for optical frequency applications[3,4] including infrared detection[5,6] and solar energy harvesting[7,8]. Integrating them into rectenna arrays[9] offers the distinct advantage over photovoltaics of harvesting IR energy during night time hours. The main challenges remain in achieving sufficient nonlinearity, high asymmetry, and low dynamic resistance[10] to achieve sufficiently high efficiency. Resonant tunneling (RT) can serve to bring further enhancement to the current asymmetry and nonlinearity[11] with demonstrated operation at THz frequencies.[12,13]

The device structure comprises of one or two dielectric layers of a few nanometer thickness sandwiched between two metal electrodes. The aim is to develop diodes with sufficiently nonlinear and asymmetric current density–voltage (*J*-*V*) characteristics, which can be achieved by the choice of the dielectrics and their thicknesses. Asymmetry

is defined as the ratio of the current (I) at positive bias to that at negative bias at certain voltage $f_{asym} = I_{+}/I_{-}$. The dynamic resistance is defined as $R_d = dV/dI$. Nonlinearity is defined as the ratio of the static to dynamic resistance $f_{NL} = (V/I)/R_d$[14] and needs to be greater than about three.[15]

In this contribution, the conduction mechanisms dominating in 4 nm thick atomic layer deposited (ALD) Al_2O_3 and Ta_2O_5 are studied in metal-insulator-metal (MIM) structures. With 1 nm of the former and 1–4 nm thickness tuning of the latter, the effect of RT on metal-insulator-insulator-metal (MIIM) diode performance is investigated experimentally by studying the effect of varying the thickness of one layer in an MIIM structure.

II. FABRICATION

Devices with lateral area of $100 \times 100\ \mu m^2$ of structures presented in TABLE I were fabricated on cleaned Corning glass substrates. The top and bottom metal layers of 50 nm thickness were deposited by thermal evaporation through a shadow mask. The Al_2O_3 and Ta_2O_5 oxides were successively deposited over the bottom electrodes by ALD at a temperature of 200 ºC using deionized water as the oxidant for Ta_2O_5 and Al_2O_3 at 0.04 s/10 s pulse/purge time, tantalum ethoxide precursor for Ta_2O_5 at 0.3 s/2 s pulse/purge time, and trimethylaluminum (TMA) precursor for Al_2O_3 at 0.02s/5s pulse/purge time. The thicknesses of the dielectric layers were measured by variable angle spectroscopic ellipsometry using a *XLS-100 J.A. Woollam* instrument. The *J-V* measurements were done in the dark using an *Agilent B1500 Semiconductor Device Analyzer* on a

temperature controlled heating stage. The voltage was swept from 0 V with 10 mV step size in negative and positive bias.

TABLE I. Device structure and layer thickness.

Structure	Bottom contact	Thickness (nm)		Top contact
		Al_2O_3	Ta_2O_5	
S1	Au	4	—	Al
S2	Al	—	4	Al
S3	Cr	1	1	Al
S4	Cr	1	2	Al
S5	Cr	1	3	Al
S6	Cr	1	4	Al

III. Material Selection

The possible tunneling mechanisms in each structure are illustrated schematically using the energy band diagrams shown in FIG. 1 considering literature values for the work functions [4.2,[16] 4.4,[16] and 5.1 (Ref. 17) eV for Al, Cr, and Au, respectively] and electron affinity, $q\chi$,[18] of 1.35 and 3.75 eV for Al_2O_3 and Ta_2O_5, respectively. These values and a dielectric constant of 10 (Ref. 19) and 25,[20] for Al_2O_3 and Ta_2O_5, respectively, have been used for all theoretical calculations. When electrons are injected from the bottom electrode (right to left on the diagrams) at negative bias, the current in single barrier structures could be driven by direct or Fowler–Nordheim (FN)[21] tunneling; the latter is depicted for the case of S2 in FIG. 1. For double dielectric structures, this could turn into one-barrier step tunneling[22] at sufficient negative bias as for S6 and S3. For opposite injection of electrons at positive bias, RT may occur in double barrier MIIM structures when the quantum well formed between the dielectrics becomes wide and deep enough to allow the formation of bound states[23] enabling resonant tunneling. It is shown

in FIG. 1(b) that these could be achieved for S6 but not S3. Al_2O_3 has a large conduction band offset with Ta_2O_5, necessary to create the quantum well, which gets wider and deeper when it is thin enough (1 nm) and when Ta_2O_5 is thick enough (4 nm).

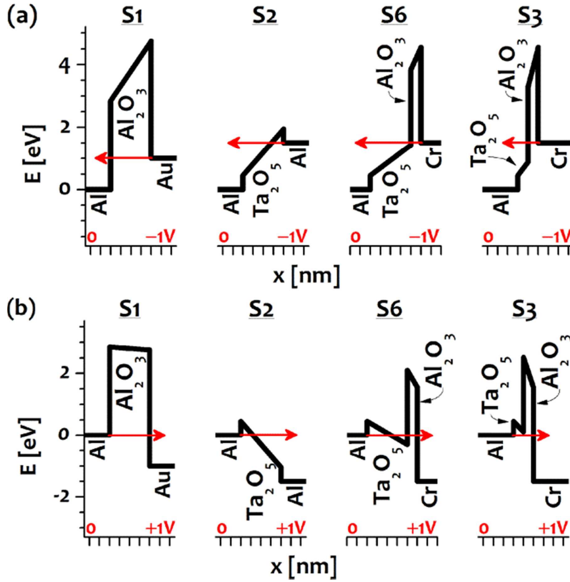

FIG. 1. (Color online) Energy band diagrams (conduction band) of four structures at −1 (a) and +1 V (b). Direction of electron injection is indicated by red arrows. Top electrode is always referred to zero. One tick on the x-axis corresponds to 1 nm.

Despite the advantage of Al work function to create a deep quantum well for RT at lower voltage, the AFM images of Fig. 2 reveal a large surface roughness of 2.8 nm, which is not smooth enough for deposition of such thin dielectric layers. The metals Cr and Au serve better as bottom electrodes due to their ultrasmooth surface roughness of 0.42 and 0.44 nm root mean squared (*RMS*) and their lower z-excursion peaks of 4.7 and 4.6 nm, respectively, which is necessary to avoid field intensification. These metals also have high melting point as compared to the bottom Al where the ALD growth of the oxides at 200 ºC on top of it might result in the formation of interfacial layer. In addition, a few nanometer thick native oxide layer growing on top of Al when exposed to air[24] is

undesired. Despite its low surface roughness, using Au with its large work function as a bottom electrode in MIIM devices increases the metal-oxide energy barrier lowering the Fermi level of the emitter electrode so that no bound states in the quantum well could be formed in the 1.5 V voltage range. The metal Cr has a work function close to that of Al and has a native oxide of very small bandgap which does not create a large conduction band offset with Ta_2O_5 as Al. It is thus chosen as the bottom electrode for resonant tunneling structures having the advantage of its ultrasmooth surface and the possibility of forming bound states in the quantum well within the applied voltage range when used in S6 structure [FIG. 1(b)]. Using a few nanometer thick Ta_2O_5 of large electron affinity (3.75 eV) and of large band offset with a 1 nm thick Al_2O_3 (2.4 eV) allows the quantum well to be tuned below the Fermi level of the emitting electrode with the applied bias.

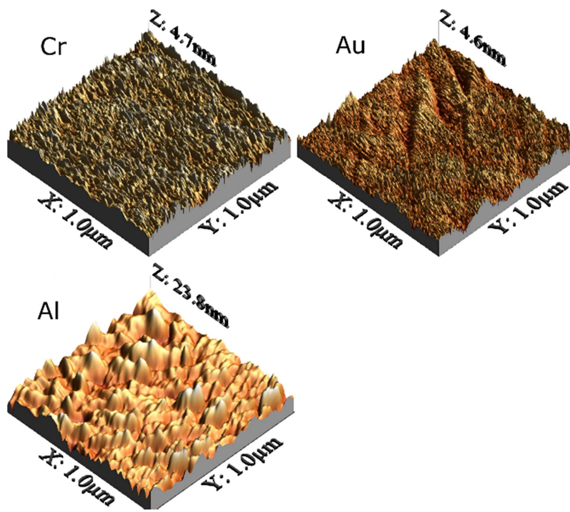

FIG. 2. (Color online) AFM images scanned at 1×1 μm^2 regions of the as-deposited bottom layers Cr, Au, and Al revealing an RMS average surface roughness of 0.42, 0.44, and 2.8 nm.

IV. RESULTS AND DISCUSSION

A. Conduction mechanisms in the individual dielectrics

The possible presence of thermally activated mechanisms is first studied individually in the single barrier structures of Al_2O_3 and Ta_2O_5. The *J-V* characteristics show temperature insensitivity for S1 [FIG. 3(a)] and strong temperature dependence for sample S2 [FIG. 3(b)]. This indicates that the 4 nm thick Al_2O_3 and Ta_2O_5 are dominated by tunneling and a thermal emission process, respectively, which is consistent with another study[25] done on 10 nm thick Al_2O_3 and Ta_2O_5. The presence of thermally activated mechanisms Schottky emission (SE) and Poole–Frenkel emission (PFE) in S2 can be examined using the logarithmic plots of I/T^2 and I/V versus $V^{1/2}$ (FIG. 4) which showed good linear fits with respect to their corresponding governing equations[26] $I_{SE} \propto T^2 exp(AV^{1/2}/kT - B)$ and $I_{PFE} \propto Vexp(AV^{1/2}/kT - B)$, respectively where A and B are constants, with a regression coefficient $R^2 > 0.995$ over the same voltage range at both polarities.

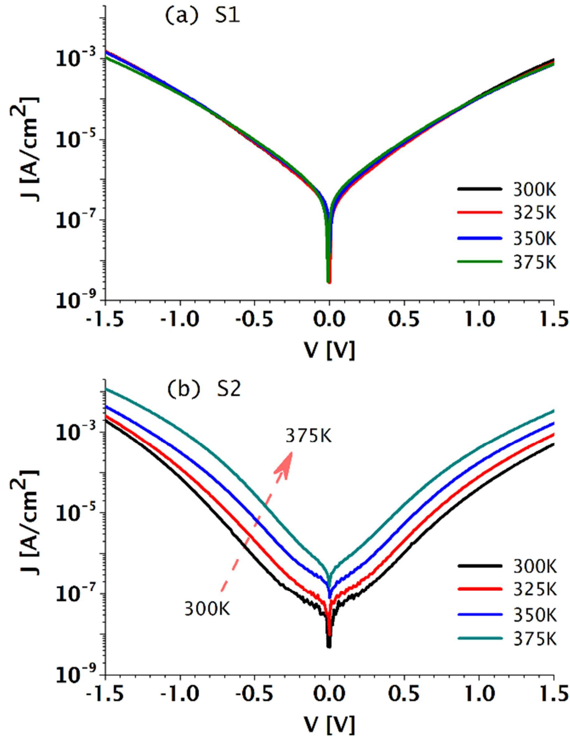

FIG. 3. (Color online) *J-V* characteristics of the MIM devices S1 (Al_2O_3) and S2 (Ta_2O_5), measured at 300, 325, 350, and 375 K.

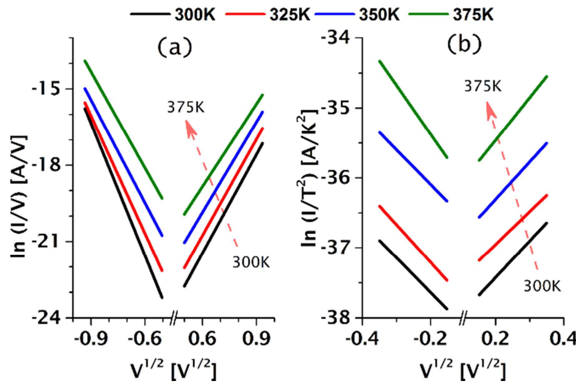

FIG. 4. (Color online) PFE (a) and SE (b) plots of the MIM device S2 (Ta_2O_5) at 300, 325, 350, and 375 K.

The average optical relative permittivity $\varepsilon_{r,opt}$, assumed to be equal to the square of the optical index of refraction n, of 50 nm thick ALD deposited Ta_2O_5 and Al_2O_3 on silicon

substrates was found to be 3.14 and 5.23, respectively, as extracted from the spectroscopic ellipsometry measurements at room temperature in the 400-1200 nm wavelength range. The equivalent dynamic relative permittivity ε_r of the 4 nm thick Ta_2O_5 extracted from the slopes of the SE plots [FIG. 4(b)] at 300 K in the 0.02-0.12 V voltage range were far larger than the optical values, and thus SE will be ruled out for this structure (S2). Only ε_r extracted from PFE plots for S2 was self-consistent with $\varepsilon_{r,opt}$ using a trap compensation factor[27] (CF) multiplied by kT in PFE equation ranging[28,29] from 1 to 2. This indicates the dominance of PFE in the 4 nm thick Ta_2O_5 ranging widely from 0.25 to 1.5 V at both polarities (TABLE II).

Despite the work function dissimilarity of 0.9 eV (Ref. 16) in S1, no noticeable asymmetry could be observed due to the large barrier across the low-χ Al_2O_3 preventing the occurrence of FN tunneling within the applied voltage range (FIG. 1).

TABLE II. Extracted CF when $\varepsilon_{r,\mathrm{PFE}}$ is matched to $\varepsilon_{r,opt}$ (CF_m), the voltage range in which PFE fitting is done (V_{PFE}), and the trap depth at zero bias φ_{t0} for the 4 nm thick Ta_2O_5 at negative (–) and positive (+) polarities at 300 K.

Bias	CF_m	V_{PFE} (V)	$q\varphi_{t0}$ (eV)
–	1.35	0.25–1.5	0.9
+	1.81		0.53

The linear fit of the Arrhenius plots (FIG. 5) is used to extract the activation energy (E_a) (FIG. 6) associated with the dominant oxide trap in S2, such that $I_{PFE} \propto V exp(-E_a/kT)$, where k is the Boltzmann constant and T is the absolute

temperature. The average trap depth at zero bias φ_{t0} extracted at positive bias for the 4 nm thick ALD Ta_2O_5 (TABLE II) was equal to the 0.53 eV extracted for 10 nm thick ALD Ta_2O_5 in other studies.[25,30] PFE is a bulk limited process and should ideally be independent of voltage polarity. The polarity dependence apparent in FIG. 3(b), therefore, could be related to the difference in interfacial roughness of the top and bottom electrodes, which intensifies the electric field leading to lowering of the effective barrier height and hence increasing the current.[31]

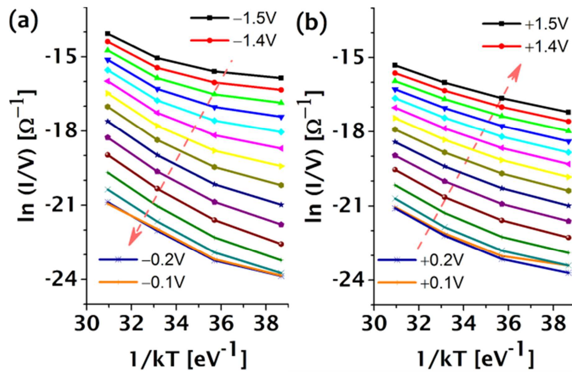

FIG. 5. (Color online) Arrhenius plots of the MIM device S2 from 0 to +1.5 (a) and to −1.5 V (b) at a 0.1 V step voltage.

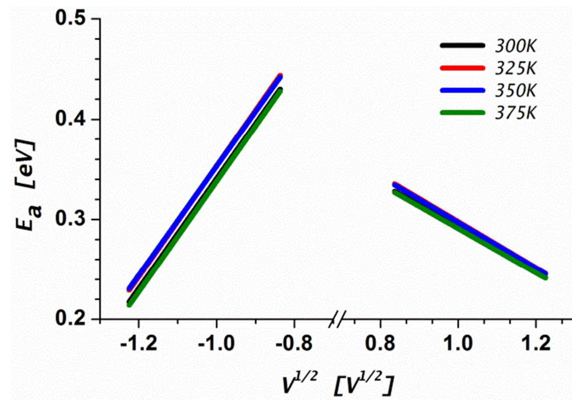

FIG. 6. (Color online) Activation energy (E_a) versus square root of voltage plots for the MIM device S2 at 300, 325, 350, and 375 K.

B. Barrier tuning of double dielectric diodes

The effect of varying the individual layer thickness of Ta_2O_5 with a 1 nm thick Al_2O_3 dielectric can be observed in the rectifying characteristics shown in FIG. 7. It should be noted that the quantum well between the two dielectric layers becomes wider and deeper by either increasing the applied voltage or the thickness of the high-χ oxide (S6) giving rise to bound states in the quantum well.[32] The abrupt increase in the *J-V* plots [FIG. 7(a)] at positive bias of 0.32 V for the 4 nm thick Ta_2O_5 oxide could be attributed to RT. This possibility is supported by the band diagrams of FIG. 1(b) which indicate the probable occurrence of RT at positive bias, when the energy of a bound state in the well is matched to the states neighboring the Fermi level of the top Al charge injecting electrode.[33] This provides further evidence that the noticeable improvement in asymmetry (*FIG. 7.b*) and nonlinearity [FIG. 7(c)] for S6 is associated with RT.

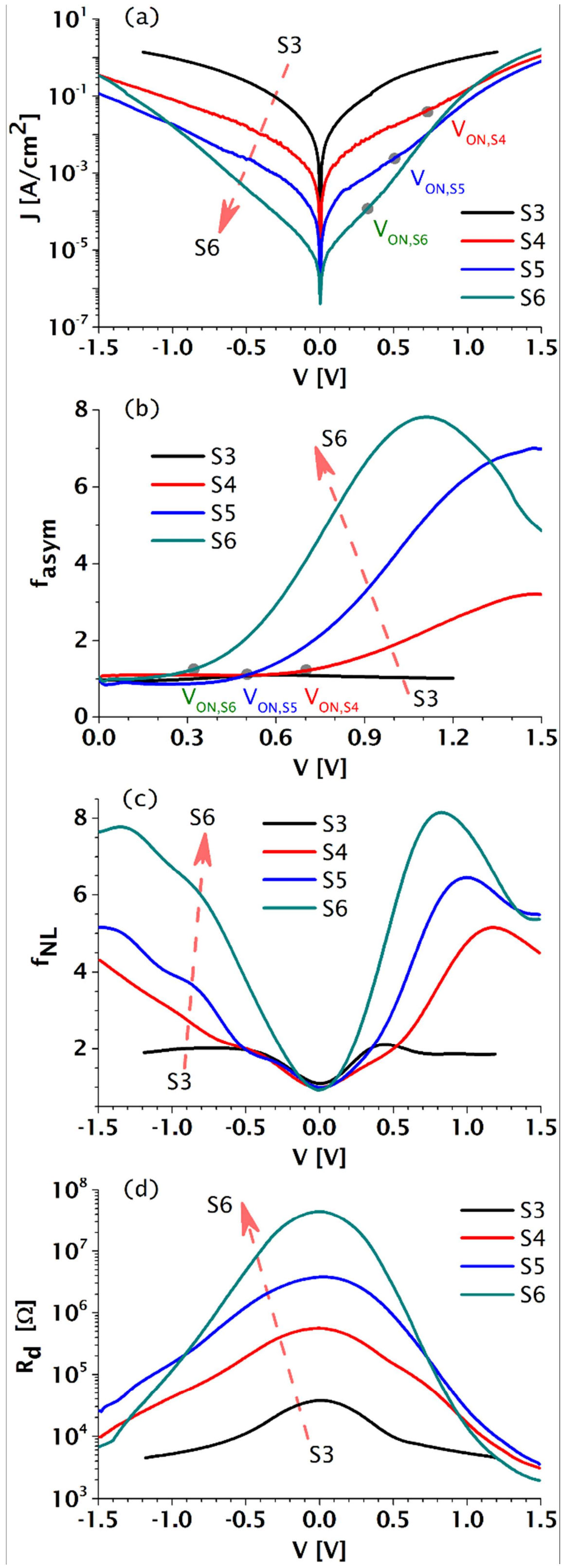

(a)
S3
S6
V_ON,S4
V_ON,S5
V_ON,S6
S3
S4
S5
S6
J [A/cm²]
V [V]
(b)
S6
S3
S3
S4
S5
S6
f_asym
V_ON,S6
V_ON,S5
V_ON,S4
V [V]
(c)
S6
S3
S3
S4
S5
S6
f_NL
V [V]
(d)
S6
S3
S3
S4
S5
S6
R_d [Ω]
V [V]

FIG. 7. (Color online) Rectifying characteristics of the MIIM devices (S3, S4, S5, and S6) showing the: (a) *J*-*V* characteristics, (b) asymmetry, (c) nonlinearity, and (d) dynamic resistance.

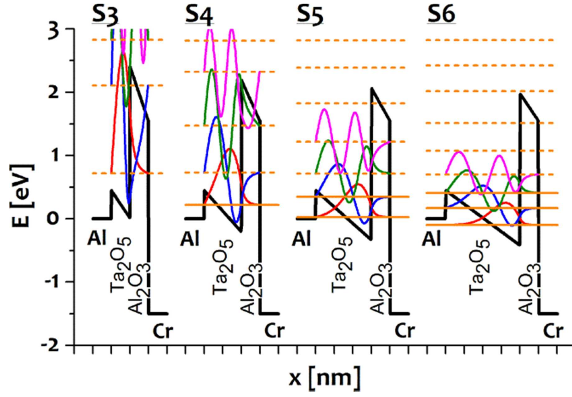

FIG. 8. (Color online) Simulated conduction band diagrams at +1.5 V showing 0, 1, 2, and 3 bound states (solid lines) for S3, S4, S5, and S6, respectively, using a work function difference of 0.2 eV (Ref. 16). One tick on the x-axis corresponds to 1 nm.

Sample S3 shows inadequate nonlinearity and asymmetry because the width of the quantum well in the device with 1 nm thick Ta_2O_5 is insufficient to accommodate a bound state in the range of the applied voltage [FIG. 1(b)]. FIG. **8** shows the simulated conduction band diagrams, the wave function inside the dielectrics (sinusoidal waves), and the bound states for S3–S6 structures using an in-house model.[32,34] The first bound state is predicted to be formed at an applied voltage of 0.98, 0.57, and 0.44 V for S4, S5, and S6, respectively. Briefly, we use the tunneling current equations and Tsu-Esaki method[35] to calculate the bound states in the quantum well within the conduction band of Ta_2O_5. We calculate the transmission probability by the transfer matrix method (TMA), that is, solving the time independent Schrödinger equation for each slice of the Tsu-Esaki multibarrier oxide. The transmission probability is then integrated in the energy domain,

applying the Fermi-Dirac statistics for occupancy of electrons in the metal contacts, to calculate the current density.

In order to observe resonant tunneling, the quantum well (FIG. 8) needs to be sufficiently wide and deep to accommodate at least one bound state. The model does not take into consideration the charge trapping predicted from the domination of PFE in the high-κ Ta_2O_5 of defect nature. Other possibilities to explain the abrupt rise in the *J*-*V* characteristics are stress-induced leakage current[36] and soft breakdown.[37] However, as no such rise in current could be observed for the MIM structures (S1–S2), these mechanisms are unlikely to explain that observed for the MIIM structures (S3–S6) fabricated at similar conditions.

A voltage V_{ON} is defined as the point at which the current abruptly increases or at the knee in the asymmetry plots. For S4, S5, and S6, V_{ON} is found to be 0.71, 0.5, and 0.32 V at positive bias in reasonable agreement with the theoretical prediction of the formation of a bound state. The decrease in V_{ON} with Ta_2O_5 thickness is consistent with the associated increase in the depth of the quantum well at positive bias as illustrated in FIG. 8. The larger current observed at positive bias for S4, S5, and S6 indicates that the overall asymmetry is regulated by the dominance of RT at positive bias over other conduction mechanisms. The effect of resonant tunneling is enhanced in structure S6 with a quantum well accommodating a number of bound states, at a certain voltage, larger than that in other MIIM structures (FIG. 8). For this device, the increase in nonlinearity [FIG. 7(c)] and the drop in dynamic resistance [FIG. 7(d)] were steeper at positive bias, where RT occurs [FIG. 1(b)], than at negative bias, where step tunneling occurs [FIG. 1(a)], indicating the advantage of the prior mechanism in rectification. As the Ta_2O_5 thickness

is varied, a trade-off is apparent between the asymmetry, nonlinearity, and low V_{ON} and the dynamic resistance [FIG. 7(d)], which needs to be reduced for impedance matching in the THz rectenna. Accordingly, the choice of an optimum RT structure should take into consideration this trade-off depending on the application.

V. SUMMARY AND CONCLUSIONS

Atomic layer deposited Ta_2O_5 and Al_2O_3 oxides were used in single and double barrier structures to identify and optimize their rectifying performance. The dominant conduction mechanisms in 4 nm thick layers of Al_2O_3 and Ta_2O_5 were shown to be tunneling in the former and PFE in the latter. There was self-consistent evidence for resonant tunneling in double dielectric diodes arising from the noticeable enhancement in nonlinearity and asymmetry in agreement with the theoretical modeling. The effect of RT was tuned according to the individual thickness of the Ta_2O_5 layer resulting in a noticeable improvement in rectification as the quantum well becomes wider such as to accommodate more bound states. Enhanced rectifying characteristics were observed at a turn-on voltage as low as 0.32 V. It is feasible that exploitation of work function engineering can further reduce the turn-on voltage to allow the zero-bias rectification[34] necessary for energy harvesting in rectenna structures.

ACKNOWLEDGMENTS

This work has been partly funded by EPSRC, UK, under Project No. EP/K018930/1. The authors thank the collaborating partners: J. Wrench and P. R. Chalker from the Centre for Materials and Structures for the ALD. I.N.N. acknowledges the University of Liverpool and National Tsing Hua University for provision of a studentship.

[1]S. Hall, I. Z. Mitrovic, N. Sedghi, Y. C. Shen, Y. Huang, and J. F. Ralph, *Functional Nanomaterials and Devices for Electronics, Sensors and Energy Harvesting* (Springer, Cham, Switzerland, 2014), p. 241.

[2]E. H. Hauge and J. A. Støvneng, Rev. Mod. Phys. 61, 917 (1989).

[3]G. M. Elchinger, A. Sanchez, C. F. Davis, and A. Javan, J. Appl. Phys. 47, 591 (1976).

[4]M. Sarehraz, "Novel rectenna for collection of infrared and visible radiation," Ph.D. thesis (Univerity of South Florida, 2005).

[5]P. C. D. Hobbs, F. R. Libsch, N. C. LaBianca, R. B. Laibowitz, and P. P. Chiniwalla, Opt. Express 15, 16376 (2007).

[6]S. Grover, O. Dmitriyeva, G. Moddel, and M. J. Estes, IEEE Trans. Nanotechnol. 9, 716 (2010).

[7]M. Dagenais, K. Choi, F. Yesilkoy, A. N. Chryssis, and M. C. Peckerar, Proc. SPIE 7605, 76050E (2010).

[8]S. Bhansali, S. Krishnan, E. Stefanakos, and D. Y. Goswami, AIP Conf. Proc. 1313, 79 (2010).

[9]Y. Huang, S. Hall, and Y. Shen, UK patent 2484526 (A) (18 April 2012).

[10]G. Moddel and S. Grover, *Rectenna Solar Cells* (Springer, New York, 2013).

[11]S. Grover and G. Moddel, Solid State Electron. 67, 94 (2012).

[12]M. Feiginov, K. Hidetoshi, S. Safumi, and A. Masahiro, Appl. Phys. Lett. 104, 243509 (2014).

[13]T. C. L. G. Sollner, W. D. Goodhue, P. E. Tannenwald, C. D. Parker, and D. D. Peck, Appl. Phys. Lett. 43, 588 (1983).

[14]P. Maraghechi, A. Foroughi-Abari, K. Cadien, and A. Y. Elezzabi, Appl. Phys. Lett. 100, 113503 (2012).

[15]B. Berland, NREL Subcontractor Final Report, Littleton Report No. NREL/SR-520-33263, 2003.

[16]C. J. Smithells, W. F. Gale, and T. C. Totemeier, *Smithells Metals Reference Book*, 8th ed. (Elsevier Butterworth-Heinemann, Oxford, England; Burlington, MA, 2004), p. 18.

[17]S. M. Sze and K. K. Ng, *Physics of Semiconductor Devices*, 3rd ed. (Wiley-Interscience, Hoboken, NJ, 2007), p. 137.

[18]R. G. Southwick, A. Sup, A. Jain, and W. B. Knowlton, IEEE Trans. Device Mater. Reliab. 11, 236 (2011).

[19]D. A. Buchanan *et al.*, International Electron Devices Meeting (2000), p. 223.

[20]K. Kukli, M. Ritala, and M. Leskela, J. Electrochem. Soc. 142, 1670 (1995).

[21]R. H. Fowler and L. Nordheim, Proc. R. Soc. London A 119, 173 (1928).

[22]Y. Matsumoto, T. Hanajiri, T. Sugano, and T. Toyabe, Jpn. J. Appl. Phys., Part 1 35, 1126 (1996).

[23]N. Sedghi, J. F. Ralph, I. Z. Mitrovic, S. Hall, and P. R. Chalker, Appl. Phys. Lett. 102, 092103 (2013).

[24]R. Winston Revie and H. Henry Uhlig, *Corrosion and Corrosion Control: An Introduction to Corrosion Science and Engineering*, 4th ed. (Wiley, Hoboken, NJ, 2008), p. 383.

[25]N. Alimardani, S. W. King, B. L. French, T. Cheng, B. P. Lampert, and J. F. Conley, Jr., J. Appl. Phys. 116, 024508 (2014).

[26]S. M. Sze, *Physics of Semiconductor Devices* (Wiley-Interscience, New York, 1969), p. 496.

[27]W. R. Harrell and J. Frey, Thin Solid Films 352, 195 (1999).

[28]A. G. Milnes, Deep Impurities in Semiconductors (Wiley, New York, 1973), p. 99.

[29]R. A. Ongaro and A. A. Pillonnet, Rev. Phys. Appl. 24, 1085 (1989).

[30]N. Alimardani, J. M. McGlone, J. F. Wager, and J. F. Conley, J. Vac. Sci. Technol., A 32, 01A122 (2014).

[31]C. W. Miller, Z. P. Li, I. K. Schuller, and J. Åkerman, Appl. Phys. Lett. 90, 043513 (2007).

[32]Z. Wang, J. Ralph, N. Sedghi, I. Z. Mitrovic, and S. Hall, J. Vac. Sci. Technol., B 31, 021209 (2013).

[33]L. L. Chang, L. Esaki, and R. Tsu, Appl. Phys. Lett. 24, 593 (1974).

[34]N. Sedghi, I. Z. Mitrovic, J. F. Ralph, and S. Hall, *WoDiM*, Cork, Ireland (2014).

[35]R. Tsu and L. Esaki, Appl. Phys. Lett. 22, 562 (1973).

[36]E. Rosenbaum and L. F. Register, IEEE Trans. Electron Devices 44, 317 (1997).

[37]M. Depas, T. Nigam, and M. M. Heyns, IEEE Trans. Electron Devices 43, 1499 (1996).